SUPPLEMENTARY INFORMATION

Methods and Materials

In vivo studies

The animal studies were performed by Mayo Clinic (and approved by the Mayo Institutional Animal Care and Use Committee) using three patient derived xenograft (PDX) lines: GBM12, GBM22 and GBM84 (PDX National Resource, Mayo Clinic). Athymic nude mice were used and the xenografts were implanted in the flank using 1 million cells (for GBM22) or 2 million cells (for GBM12 and 84) per animal in PBS. The tumors grew for 14 days (GBM12), 25 days (GBM84) and 16 days (GBM22). An adavosertib (Selleck) suspension in 0.5% methocel in water was used for treating the animals with a dose of 50 mg/kg, 15 mg/kg or vehicle (5 animals per condition, per PDX). Each animal received 9 doses BID PO and were harvested 2h after the last treatment at Cmax.

Clinical trial specimens

The clinical trial specimens were obtained from 6 different patients with recurrent GBM enrolled on the surgical arm of a phase I study of adavosertib (MK-1775 or AZD1775) led by the Adult Brain Tumor Consortium (ABTC), approved by the human investigations committee at Dana-Farber / Harvard Cancer Center, and registered on clinicaltrials.gov (NCT01849146). Informed written consent was obtained from each participant. The accepting criteria included participants with recurrent GBM that required surgery for tumor removal. Participants had to take a daily dose of adavosertib four days prior to surgery and they were assigned to a treatment group receiving 200 mg (cases b and e) or 425 mg (cases a, c, d and f) for 5 consecutive days. During

surgery, a portion of the tumor was collected from contrast enhancing and non-contrast enhancing areas for the purpose of this study, and specimens were immediately flash frozen and kept at -80°C until analysis.

Tissue sample preparation

Frozen mouse specimens and clinical tissue specimens were stored at -80°C, and placed in a Microm HM550 cryostat (Thermo Scientific™) at -25°C for 1 hour prior to sectioning. Cryo-sections of 10-µm thickness were thaw mounted onto indium tin oxide (ITO)-coated glass slides (Bruker Daltonics, Billerica, MA) and consecutive sections were mounted on regular microscopy glass slides to perform hematoxylin and eosin (H&E) staining. Optical images of the slides were acquired using a scanner with 3200 dpi image resolution, and then ITO slides were coated with DHB (160 mg/mL in 70:30 MeOH:0.1% TFA and 1% DMSO) using an automated matrix applicator (TM-sprayer, HTX imaging, Carrboro, NC) under the following conditions: 2 passes, 0.18 mL/min flow rate, 75°C, 10 psi nitrogen pressure, followed by recrystallization at 85°C with acetic acid 5%.

MALDI FT-ICR MSI

Mass spectrometry imaging analysis was performed using a Matrix Assisted Laser Desorption Ionization (MALDI) ionization source and 9.4 Tesla SolariX XR Fourier Transform Ion Cyclotron Resonance (FT-ICR) mass spectrometer (Bruker Daltonics, Billerica, MA). Spectra were acquired using the positive ion mode and a 1 kHz Smartbeam™ laser. The laser pixel raster size was set to 100 µm for the flank tumors and 30 µm for the clinical trial specimens, performing 250 accumulated laser shots per spot with 1000 Hz of frequency, FID 1.1185s. The

acquisition mass range was *m/z* 155-3000, and the analysis was performed using continuous accumulation of selected ions (CASI) mode, with a window between *m/z* 495-665. Spectra were externally calibrated using a small-molecule calibration standard solution. The resolution power used was of 150,000.000 (*m/z* 501.27209 - adavosertib). The software used for acquisition were FTMS Control and flex Imaging 5.0 (Bruker Daltonics, Germany), and SCiLS 2019a was used for data visualization and treatment. Tentatively assigned molecules using HMDB and LipidMaps are in table S6.

Quantification of drug concentration by MALDI FT-ICR MSI

For the drug quantification in the flank tumors, a mimetic model was made using gelatin molds containing brain homogenate and different concentrations of adavosertib standard[1]. The tissue homogenate was prepared with concentrations of adavosertib of 20, 15, 10, 5, 2, 1 μM and a blank homogenate was also prepared. Pixel ion intensity in the ROI was considered a measure of drug concentration to build the calibration curve. The quantification method was selective to adavosertib, not presenting any other ion with the same *m/z*, with the resolving power of the FT-ICR MS described above for the drug. Visual inspection of the spectra confirmed the selectivity of the method. The linearity range was between 1-20 μM with a correlation value R^2= 0.9952. Precision and accuracy were calculated using five sections of tissue mimetic homogenates mounted on an ITO slide, and analyzed by MALDI FT-ICR MSI, with the parameters described in the previous item. These parameters were calculated at low (1 μM), medium (10 μM) and high (20 μM) drug levels (table S7).

Phosphoproteomics

Tumor Tissue Processing

Frozen tumors were homogenized using the VWR 200 Homogenizer in ice-cold 8M urea. Protein concentration was measured by Bicinchoninic acid assay (BCA) (Pierce) by taking a small aliquot from the soluble fraction of the lysate. Proteins were reduced with 10 mM dithiothreitol (Sigma) for 1 hour at 56 °C followed by alkylation of thiols with 55 mM iodoacetamide (Sigma) for 1 hour in dark at room temperature. Lysates were diluted 4-fold with 100 mM ammonium acetate at pH 8.9 before digesting overnight with 1 µg sequencing grade trypsin (Promega) per 50 µg of protein at room temperature. Digestion reaction was quenched by acidifying the samples with acetic acid. Peptides were desalted on a C18 Sep-Pak Plus cartridges (Waters) and eluted with 40% acetonitrile (Sigma) in 0.1% acetic acid (Sigma). Eluates were concentrated in SpeedVac centrifuge. Aliquots of 400 µg (of starting protein) were lyophilized and stored at -80 °C.

TMT Labeling

Lyophilized peptides were labeled with or TMT6-plex or TMT10-plex labeling kits (Thermo Fisher Scientific). To allow comparison of data from two multiplex analyses, a common sample was used in two different TMT multiplex runs. Each peptide aliquot was resuspended in 70 µL ethanol and 30 µL of 0.5 M triethylammoniumbicarbonate at pH 8.5, followed by incubating with TMT reagent resuspended in 30 µL anhydrous acetonitrile for 1 hour at room temperature. The samples were pooled together and dried down in a SpeedVac.

Phosphopeptide enrichment

Phosphopeptides were enriched sequentially using immunoprecipitation (IP) and High-Select Fe-NTA Phosphopeptide Enrichment kit (Pierce). TMT labeled samples resuspended in IP buffer (100 mM Tris-HCl, 1% Nonidet P-40 at pH 7.4) were incubated with protein G agarose beads conjugated with 12 µg 4G10 (Millipore), 6 µg pY100 (Cell Signaling Technology) and 6 µg PT-66 (Sigma) overnight at 4 °C. The supernatant was saved for subsequent peptide analysis. The beads were washed once with IP buffer and thrice with rinse buffer (100 mM Tris-HCl at pH 7.4). Peptides were eluted twice, each with 25 µL of 0.2% trifluoroacetic acid (TFA) for 10 mins at room temperature. For ATM/ATR substrate analysis, supernatant from phosphotyrosine IP was subjected to a secondary IP with PTMScan Phospho-ATM/ATR Substrate Motif kit (Cell Signaling Technology). After overnight incubation, peptides were eluted with 0.2% TFA and subjected to secondary Fe-NTA spin column enrichment.

Phosphopeptides from the IP eluate were enriched with High-Select Fe-NTA enrichment kit according to manufacturer's protocol with following modifications. After washing the Fe-NTA spin columns, the beads were resuspended in 25 µL of binding/washing buffer. Peptides eluted from IP were incubated with Fe-NTA beads for 30 minutes. Beads were rinsed thrice with binding/washing buffer and once with HPLC grade water. Peptides were then eluted twice with 20 µL of elution buffer into a clean 1.7 mL Eppendorf tube. Samples were dried in vacuum centrifuge until 1-5 µL of sample remained. Peptides were resuspended in 10 µL of 5% acetonitrile in 0.1% formic acid and loaded directly into an inhouse packed analytical capillary column (50 µm ID x 10 cm) packed with 5 µm C18 beads (YMC gel, ODS-AQ, AQ12S05).

LC-MS/MS

Peptides were separated on an Agilent 1260 using a 140 min gradient ranging from 0% to 70% acetonitrile in 0.2 M acetic acid at a flow rate of 0.2 mL/min. With a flow split of approximately 10,000:1, the final electrospray flow rate was estimated to be 20 nL/min. Peptides were analyzed using a Q Exactive HF-X Hybrid Quadrupole-Orbitrap mass spectrometer (Themo Fisher). The instrument was operated in data-dependent acquisition mode with *m/z* ranging from 350-2000 at 60,000 resolution. The AGC target for MS1 scans was set to 3×10^6 and maximum injection time of 50 ms. Up to 15 most abundant ions were isolated (0.4 m/z isolation width) and fragmented (collisional energy (CE):33%) by higher energy collision dissociation (HCD) with a maximum injection time (IT) of 350 ms, AGC target of $1x10^5$ and resolution of 45,000.

To correct for slight variation in sample amount for each of the TMT channel, approximately 30 ng of the supernatant from IP was loaded onto an inhouse packed precolumn (100 µm ID x 10 cm) with 10 µm C18 beads (YMC gel, ODS-A, AA12S11). The precolumn was connected in series with an analytical column, and peptides were analyzed on Q Exactive Plus mass spectrometer (Themo Fisher) and acquired using the sofware Xcalibur (Themo Fisher). Peptides were eluted using a 70 min gradient ranging from 0% to 70% acetonitrile in 0.2 M acetic acid. Instrument settings were similar to those of HF-X with following changes: MS1 scans were performed at resolution of 70,000. Top 10 abundant ions were isolated with maximum IT of 150 ms.

Peptide identification and quantification

Raw MS data files were processed with Proteome Discoverer version 2.2 (Thermo Fisher Scientific). MS spectra were searched against the human SwissProt database using Mascot version 2.4 (Matrix Science). TMT reporter quantification was extracted using Proteome

Discoverer. MS/MS spectra were searched with mass tolerance of 10 ppm for precursor ions and 20 mmu for fragment ions. Minimum peptide length was set to six amino acids, and up to two tryptic miscleavages were allowed. Fixed modifications were included for cysteine carbamidomethylation, TMT-labeled lysine and TMT-labeled peptide N-termini. Phosphorylation of serine, threonine, tyrosine and oxidation of methionine were searched as dynamic modifications. Peptide spectrum matches (PSMs) with mascot ion score > 18 and isolation interference of < 30% were used for downstream analysis. Phosphorylation sites were localized using ptmRS module on Proteome Discoverer. Only PSMs with >95% localization probability for all sites were included for downstream analysis. For ATM/ATR substrates, peptides that contain 'SQ' or 'TQ' motif were included for analysis. TMT reporter ion intensities were summed for each phosphopeptide. Phosphopeptide quantification was normalized using the median relative quantification of peptides with ion score >25 from the supernatant analysis to correct for small variation in sample input. For each phosphopeptide, relative quantification was represented as a ratio between TMT ion intensities of each analyzed tumor and the average of vehicle treated tumors. For clinical samples, TMT ion intensities were mean normalized across individual phosphopeptides.

PLSR and Statistical Analysis

Phosphoproteomics was performed on frozen tumors as described previously[2] with few modifications. Proteomics data were analyzed and visualized using MATLAB or corresponding Python packages. One tumor from GBM84 line treated with 15 mg/kg was dropped from analysis because of overall ultra-low level of phosphorylation. Tumors used as common normalization channels to combine two TMT runs were not used for computational analyses

resulting in total of 13, 9 and 13 animals for GBM12, GBM22 and GBM84 lines, respectively. For PLSR analysis, adavosertib levels from MALDI-MSI and proteomics data were presented as log2 fold change over the mean of vehicle treated group. PLS regression was performed using the scikit-learn package in Python[3]. Initial PLS models were built to assess the fit of the model (calibration) and identify optimal number of principal components. Model built with optimal number of components was cross-validated using the leave-one-out procedure, where each treatment was individually withheld from the training set, and withheld treatment was predicted using the model. Coefficient of determination (Q^2) between the measured drug levels and cross-validation predicted drug levels was calculated using r2_score function in scikit-learn package. Peptides contributing most to the model were identified using Variable Importance in Projection (VIP) score as previously described[4]. Protein networks were obtained using the STRING database[5].

Tissue-based Cyclic Immunofluorescence (t-CyCIF)

Tissue samples and slide preparation

Same specimens used for MSI and phosphoproteomics were analyzed by t-CyCIF.

The t-CyCIF validation of FF specimens compared to FFPE was performed using a GBM22 PDX flank model, prepared using the same procedure as described previously on the in vivo studies item. In this case, for t-CyCIF validation purposes, after the tumors were harvested they were cut in half: One half of the tumors was used to generate formalin-fixed paraffin-embedded (FFPE) blocks, while the other half of the tumors was flash frozen (FF) in liquid nitrogen.

FFPE sections were prepared at 5 μm thickness and mounted onto Superfrost Plus microscope slides, stored at 4 °C for subsequent t-CyCIF, while flash frozen sections of 10 μm thickness using the same type of glass slides and stored at -80 °C for subsequent t-CyCIF.

Slide Pretreatment

For FFPE slides, pretreatment was performed on the Leica Bond RX (Leica Biosystems) as described previously[6–9]. In brief, the FFPE slides were baked at 60 °C for 30 min, dewaxed at 72 °C with Bond Dewax Solution (Cat# AR9222, Leica Biosystems), and treated with Epitope Retrieval 1 (ER1) Solution at 100 °C for 20 min for antigen retrieval. The slides then were blocked with anti-Rabbit secondary antibody in Odyssey Blocking Buffer (Cat# 927–40150, LI-COR) at room temperature (RT) for 60 min, and then incubated with 1 ug/ml Hoechst 33342 (Cat# H3570, Life Technologies) at RT for 30 min.

For FF slides, the slides which had been stored at -80 °C, were immediately fixed using 4% PFA (Cat# HT501128, Sigma-Aldrich) at RT for 1 hour, washed with 1X TBS to remove residual PFA, and then permeabilized with 0.5% Triton X-100 at RT for 10 mins, and blocked with Odyssey buffer with secondary antibody and 1 ug/ml Hoechst 33342 at 4 degree overnight. After washing by 1X TBS, the FF slides went to following standard t-CyCIF procedure for slide staining and image acquisition as described before[6–9].

Slide staining and image acquisition

In the first cycle of antibody incubation, the slides were incubated overnight with primary antibodies at 4 degree and then with secondary antibodies for two hours at RT in the dark. We washed slides with 1X PBS, stained them with Hoechst solution, and then imaged them. The slides were photobleached in a solution of 4.5% H_2O_2 and 20mM NaOH in 1X PBS under a light

emitting diode (LED) for 1 hour at RT, and then incubated the antibodies directly conjugated to different fluorophores at 4 degree overnight, and then imaged. This process was repeated for 5-6 cycles using directly conjugated antibodies or unconjugated antibodies labelled by Zenon™ Alexa Fluor™ 647 Rabbit IgG Labeling Kit (Cat # Z25308, Thermo Fisher) according to instructions of use. All antibodies used in this study and t-CyCIF staining plan are listed in supplementary tables S3-5.

Regarding the image acquisition, prior to each cycle of imaging, slides were wet-mounted using 120 µl of 20% glycerol in PBS and 24 x 50mm glass cover slips (Cat # 48393-081, VWR). Images from each cycle of t-CyCIF were acquired using the IN Cell Analyzer 6000 (GE, USA) with the objective of 20X / 0.75 NA. The four channels imaged included DAPI channel, 488 channel, 555 channel and 647 channel were acquired simultaneously, and a 3% overlap was collected between fields of view to facilitate image stitching.

Image processing and data visualization

Ashlar was used to do BaSiC correction (both flat-field correction and dark-field correction) in the original images from each cycle acquired by IN Cell Analyzer 6000, then stitch the fields from the first imaging cycle into a mosaic and co-register the fields from successive cycles of imaging. The output is an OME-TIFF file that contains a seamless many-channel mosaic depicting the entire sample across all image cycles.

The OME-TIFF output was used to segment single cells in the images using Ilastik[10] and MATLAB (version 2018a). The OME-TIFF was cropped into 6000 x 6000 pixel regions to increase processing speed. From each cropped region, ~200 random 250 x 250 pixel regions were selected and used as training data on Ilastik to generate a probability of each pixel in the

cropped region belonging to three classes: nuclear area, cytoplasmic area, or area not occupied by a cell (background). MATLAB was then used to perform watershed segmentation on the probabilities to identify objects, or cells, and a segmentation mask was generated for each cropped region. Finally, single cell features included fluorescence intensity measurements of each antibody, morphological features, as well as spatial features were extracted using the segmentation mask.

Image J was used to draw region of interest (ROI) in DAPI montage from the OME-TIFF file to separate each sample from one slide and MATLAB (version 2018a) was used for single cell data analysis and visualization.

Multimodal integration

To enable one-to-one mapping for image registration, the first DAPI stained image was selected from the t-CyCIF datacube and used as a reference image. The non-linear transformation matrix was computed by optimizing a cost function that deforms the t-SNE image to be spatially aligned with the reference image. The cubic B-Spline model was used to capture the non-linear deformation and the statistical metric of mutual information was used as a cost function to assess the registration quality. The optimized non-linear transformation was applied on each *m/z* image to be aligned with the t-CyCIF data. The non-linear image registration was implemented using the publicly available toolbox of elastix[11]. Similar approach was used to compute another non-linear transformation matrix to integrate MSI and H&E images.

Dimensionality reduction and data visualization

The dimensionality reduction methods of t-distributed stochastic neighbor embedding (t-SNE) was used to non-linearly map the high-dimensional spectral points into two-dimensional

representation[12]. A major characteristic of t-SNE is its ability to preserve local structures that discerns spectra with minor variations which are otherwise undifferentiable if the focus is on preserving global variations[13].

Data integration – Harmony

t-CyCIF batch correction and clustering

We used the standard Harmony pipeline described in Korsunsky et all[14] to embed all t-CyCIF cells from the clinical trial datasets into an integrated space. We performed PCA on all markers, kept the top 9 PCs, which accounted for >70% of the total variation in the dataset. We then ran Harmony with parameters $\theta = 2$, enforcing diverse clustering, and $K = 50$, modeling the data with 50 soft clusters. We found that many of these 50 clusters were redundant with one another. We collapsed these 50 clusters into 6 non-redundant meta clusters and assigned each t-CyCIF cell to one of these 6 clusters.

t-CyCIF cluster marker association testing

We computed the association of harmonized t-CyCIF clusters in the clinical sample dataset with levels of t-CyCIF antibody staining intensities and MSI adavosertib concentration. To test these associations, we used linear mixed modeling implemented in the R lme4 package[15], with the following formula:

$$y \sim 0 + cluster + (1|Sample) + (1|Donor) + (1|Status)$$

The response variable y is an individual marker, either a t-CyCIF antibody or adavosertib concentration. $cluster$ is a fixed effect that denotes which harmonized t-CyCIF cluster a cell

belongs to. We include random effects for potentially confounding covariates. $Sample$ denotes the tissue slice, $Donor$ denotes the individual patient, and $Status$ denotes whether the slice was for a CE or NCE region.

To compute the differential expression of the response variable for each cluster, we computed the difference between the mean expression of the marker in a cluster ($\beta_{cluster=k}$) against the mean expression in all other clusters ($\frac{1}{N-1}\sum_{j\in[1,N],j\neq k}\beta_{cluster=j}$). For cluster k, this is encoded as a contrast vector $\gamma_k = [-\frac{1}{N-1}, \dots 1, \dots, -\frac{1}{N-1}]$, in which the k^{th} term is 1. We evaluated significance of these contrasts using Wald's approximation with a covariance matrix Σ that captures the covariance among the fixed effect βs:

$$\gamma_k\beta \sim N(\gamma_k\beta, \gamma_k\Sigma\gamma_k^T)$$

In other words, Σ models the covariance between mean expression levels (of t-CyCIF markers or adavosertib concentration) among the clusters. We estimate empirically Σ using 1000 rounds of posterior simulation with the R package arm[16].

t-CyCIF cluster differential abundance analysis

We tested whether t-CyCIF clusters were more or less abundant in the CE vs NCE regions using logistic regression, following the standard approach in single cell genomics[17]. In this model, cluster membership is a binary response variable (i.e. in the cluster or out of the cluster) and CE vs NCE is the fixed effect. As in the linear mixed effect models above, we included $Donor$ and $Sample$ as random effects.

$$\log_2 \frac{Pr(cluster = k)}{1 - \Pr(cluster = k)} \sim 1 + Status + (1|Sample) + (1|Donor)$$

We fit this model with the glmer function in lme4 and evaluated significance using Wald's approximation, described in the linear mixed modeling section above.

SUPPLEMENTARY METHODS REFERENCES

1. Groseclose MR, Castellino S. A mimetic tissue model for the quantification of drug distributions by MALDI imaging mass spectrometry. *Anal Chem*. 2013;85(21):10099-10106.

2. Dittmann A, Kennedy NJ, Soltero NL, et al. High-fat diet in a mouse insulin-resistant model induces widespread rewiring of the phosphotyrosine signaling network. *Mol Syst Biol*. 2019;15(8).

3. Pedregosa F \emphet al., Pedregosa F, Weiss R, et al. Scikit-learn: Machine Learning in Python. *J Mach Learn Res*. 2011;12(85):2825-2830.

4. Janes KA;, Albeck JG, Gaudet S;, Sorger PK. *A Systems Model of Signaling Identifies a Molecular Basis Set for Cytokine-Induced Apoptosis*.

5. Szklarczyk D, Franceschini A, Wyder S, et al. STRING v10: Protein-protein interaction networks, integrated over the tree of life. *Nucleic Acids Res*. 2015;43(D1):D447-D452.

6. Lin JR, Izar B, Wang S, et al. Highly multiplexed immunofluorescence imaging of human tissues and tumors using t-CyCIF and conventional optical microscopes. *Elife*. 2018;7.

7. Dunn IF, Du Z, Touat M, et al. Mismatch repair deficiency in high-grade meningioma: a rare but recurrent event associated with dramatic immune activation and clinical response to PD-1 blockade HHS Public Access. *JCO Precis Oncol*. Published online 2018.

8. Coy S, Rashid R, Lin JR, et al. Multiplexed immunofluorescence reveals potential PD-1/PD-L1 pathway vulnerabilities in craniopharyngioma. *Neuro Oncol*. 2018;20(8):1101-1112.

9. Du Z, Lin J-R, Rashid R, et al. Qualifying antibodies for image-based immune profiling and multiplexed tissue imaging. *Nat Protoc*. 2019;In press.

10. Sommer C, Straehle C, Kothe U, Hamprecht FA. Ilastik: Interactive learning and segmentation toolkit. In: *Proceedings - International Symposium on Biomedical Imaging*. ; 2011:230-233. doi:10.1109/ISBI.2011.5872394

11. Klein S, Staring M, Murphy K, Viergever MA, Pluim JPW. Elastix: A toolbox for intensity-based medical image registration. *IEEE Trans Med Imaging*. 2010;29(1):196-205.

12. Van Der Maaten L, Hinton G. *Visualizing Data Using T-SNE Laurens*. Vol 9.; 2008.

13. Wold S, Esbensen K, Geladi P. Principal component analysis. *Chemom Intell Lab Syst*. 1987;2(1-3):37-52.

14. Korsunsky I, Millard N, Fan J, et al. Fast, sensitive and accurate integration of single-cell data with Harmony. *Nat Methods*. 2019;16(12):1289-1296.

15. Bates D, Mächler M, Bolker B, Walker S. Fitting Linear Mixed-Effects Models Using lme4. *J Stat Softw*. 2015;67(1):1-48.

16. Gelman A, Su Y-S, Yajima M, et al. *Package "arm" Title Data Analysis Using Regression and Multilevel/Hierarchical Models*.; 2020.

17. Fonseka CY, Rao DA, Teslovich NC, et al. Mixed-effects association of single cells identifies an expanded effector CD4+ T cell subset in rheumatoid arthritis. *Sci Transl Med*. 2018;10(463).

18. Gajadhar AS, Johnson H, Slebos RJC, et al. Phosphotyrosine signaling analysis in human

tumors is confounded by systemic ischemia-driven artifacts and intra-specimen heterogeneity. *Cancer Res*. 2015;75(7):1495-1503.

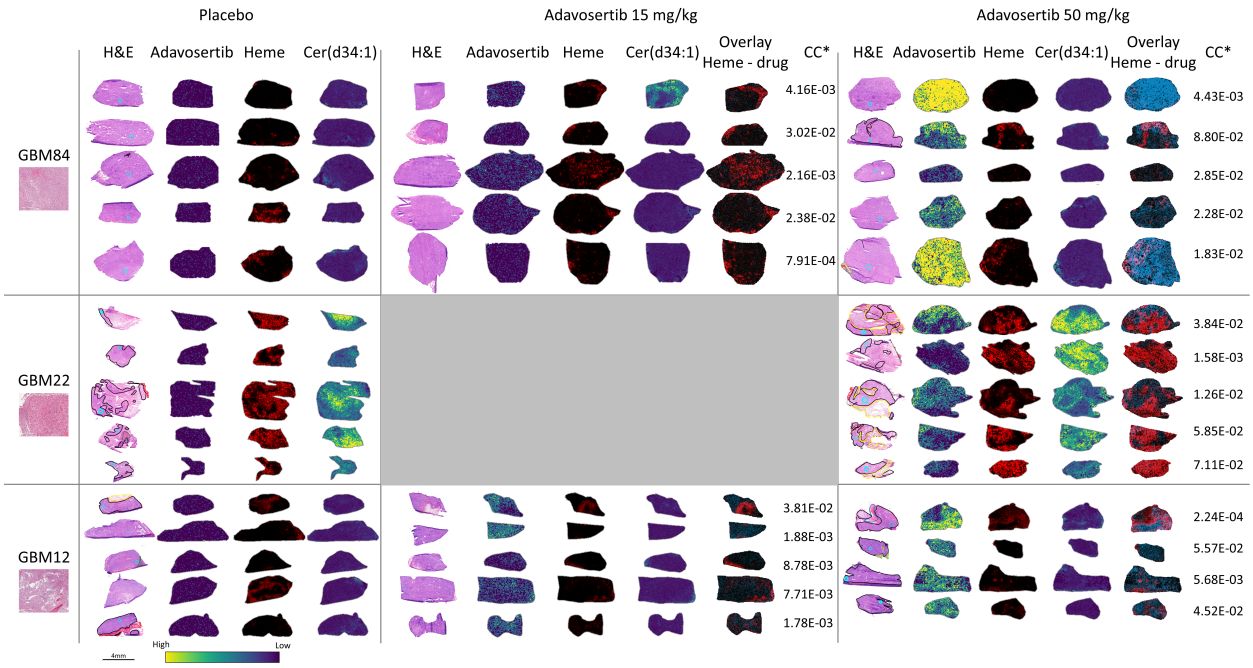

Supplementary figure S1. Distribution of adavosertib (*m/z* 501.2706) relative to heme (*m/z* 616.1768) and cer(d34:1) (*m/z* 520.5073) in flank tumors from the three GBM PDX lines treated with vehicle, 15 mg/kg and 50 mg/kg of drug. First column is a blow up of a characteristic region of the original clinical specimen of each GBM model. Delineated histological images by a neuropathologist differentiate regions of necrosis and high tumor density. For GBM84: high tumor content regions (circled in blue), necrosis (delineated in grey), infiltrated muscle (delineated in green) and tumor (delineated in black) or no delineation for dense tumor tissue sections. For GBM22: high tumor content regions (circled in blue), necrosis (delineated in yellow), infiltrated skeletal muscle (delineated in red), hemorrhage (delineated in white) and tumor (delineated in black). For GBM12: high tumor content regions (circled in blue), necrosis (delineated in grey) and tumor (delineated in black) or no delineation for dense tumor tissue sections. Distribution of adavosertib is represented by a color scale where yellow is high intensity and blue low. Heme, a cofactor of hemoglobin, is used as a marker of vasculature, also highlighting regions of hemorrhage. High intensity regions of the ceramide cer(d34:1) are displayed in yellow, coinciding with necrotic regions of GBM22, whereas lower intensity regions are represented in blue. Finally, overlay of drug (blue) and heme (red) distributions and

their corresponding correlation coefficient (CC) are represented for each specimen, showing no correlation. For high resolution image, please go to the supplementary pdf file named Figure S1.

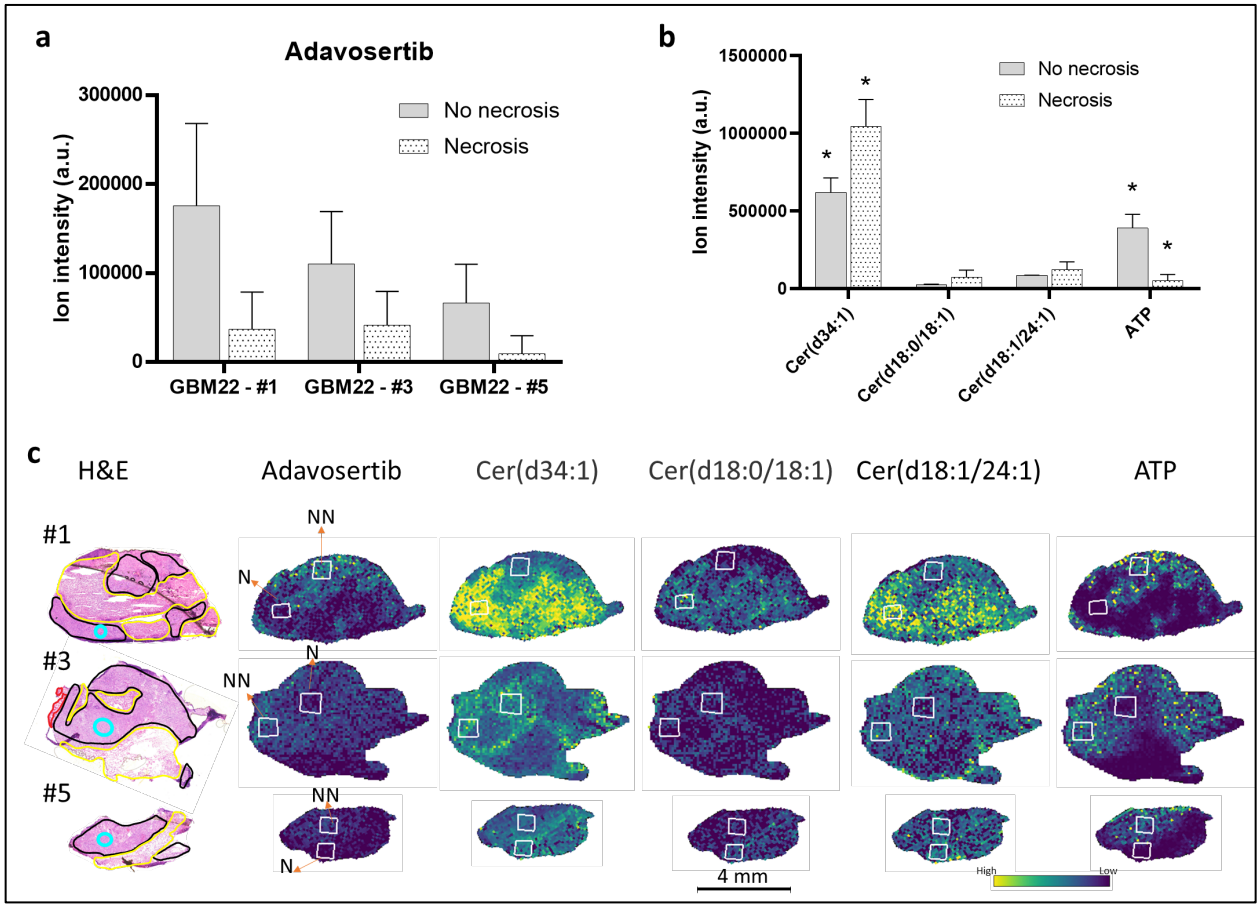

Supplementary figure S2. Correlation between drug distribution and selected molecules between non-necrotic (NN) and necrotic (N) regions of the specimens with larger necrotic areas belonging to GBM22 treated with 50 mg/kg of adavosertib. a) Box plot of the average intensities of adavosertib per pixel of NN and N regions, which are statistically different in each sample according to ANOVA ($P<0.001$). b) Box plot of the intensities of cer(d34:1) (*m/z* 520.5073), cer(d18:,/18:1) (*m/z* 548.5399), cer(d18:1/24:1) (*m/z* 630.6186) and ATP (*m/z* 508.0030) considering the average of NN and N regions in all three specimens. According to ANOVA, differences between the regions were statistically significant for cer(d34:1), higher in the N regions and for ATP displaying the opposite distribution: higher in the NN region ($P<0.001$) showing an active metabolism; c) Distribution of the drug (*m/z* 501.2706), ceramides and ATP with their corresponding histological image, displaying the NN and N regions considered for each sample. On the histological image high tumor content regions are circled in blue, necrosis is

delineated in yellow, infiltrated skeletal muscle is delineated in red and tumor is delineated in black. A representative region of each tumor is delineated by a blue circle

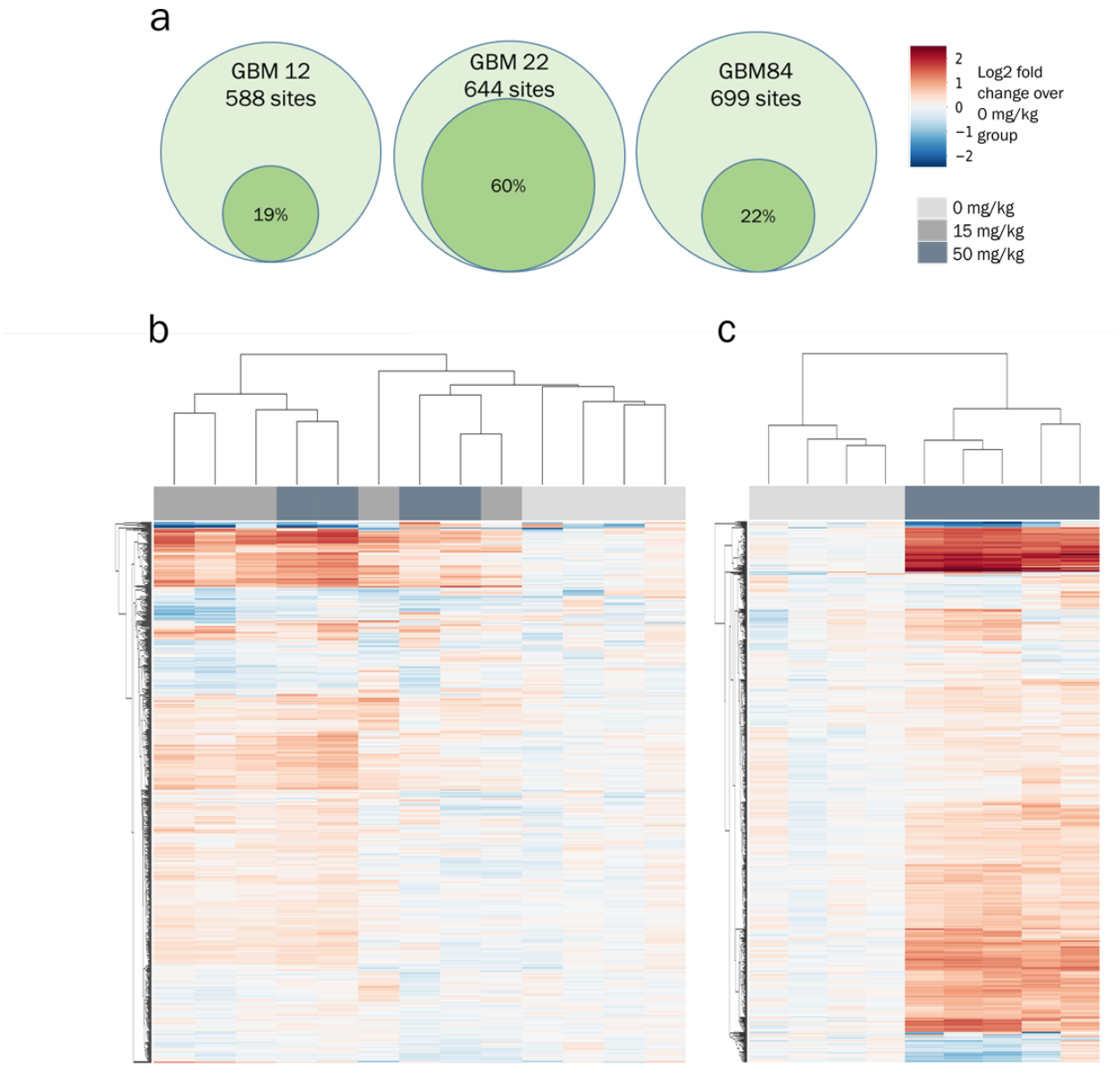

Supplementary figure S3. Phospho-SQ/TQ analysis of GBM lines. a) Total number of sites and percentage (shaded dark) of pSQ/TQ peptides showing significant increase in phosphorylation in GBM12, GBM22 and GBM84. Peptides with significant increase were identified with $p < 0.05$ (student's t-test) between vehicle and 50 mg/kg treated tumors. HCA of phosphorylation levels of pSQ/pTQ containing peptides in b) GBM12 and c) GBM22 PDX tumors treated with different doses of adavosertib. Phosphorylation levels are shown as log2 fold change over the average of vehicle treated tumors.

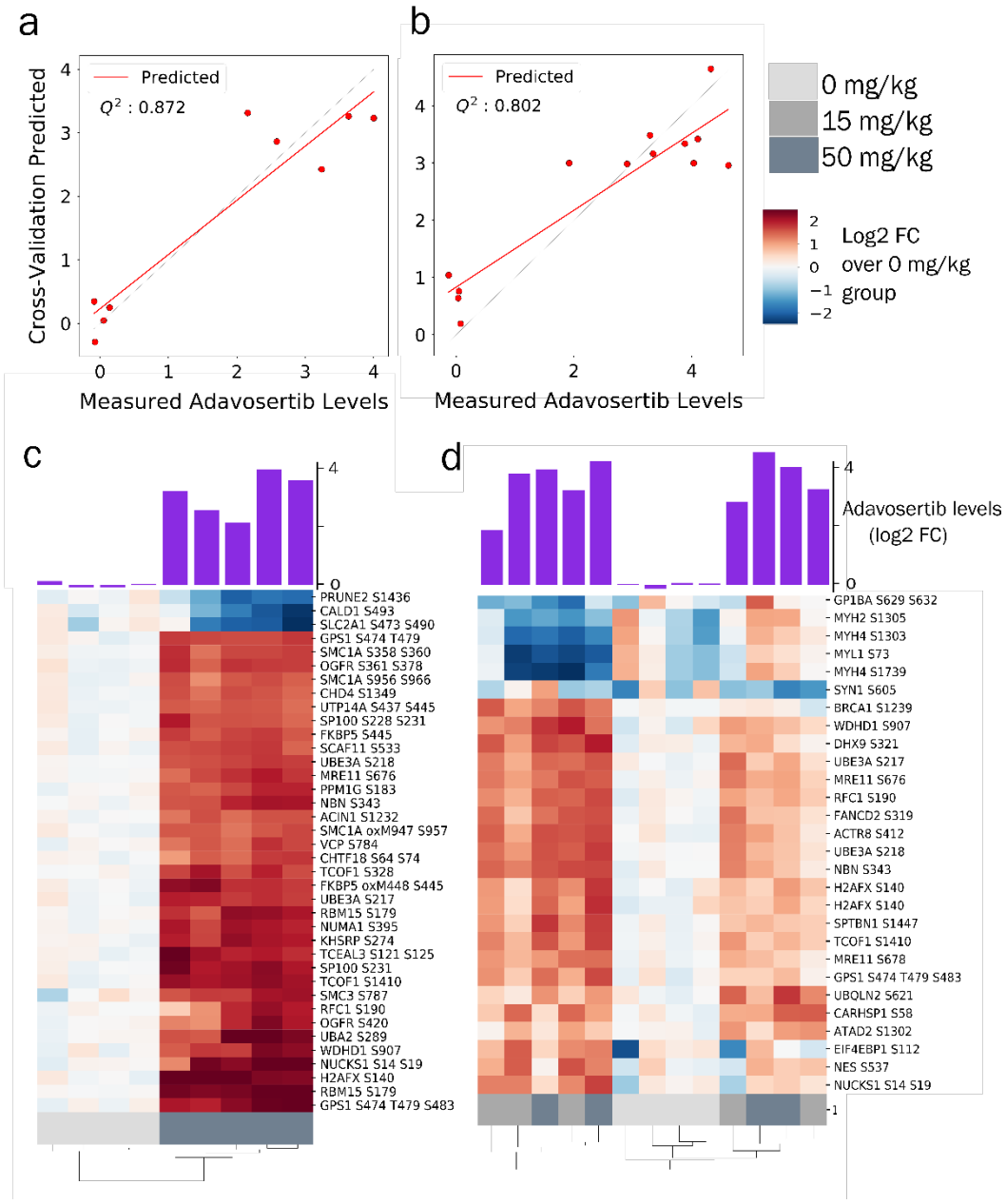

Supplementary figure S4. PLSR analysis of GBM12 and GBM22 lines. Correlation plot of measured and predicted adavosertib levels from a cross-validated model for (a) GBM22 and (b) GBM12. HCA of pSQ/pTQ sites with VIP score > 2 in models built for (c) GBM22 and (d) GBM12. A barplot with measured drug levels is overlaid on top of the clusters. Measured drug levels and phosphorylation levels are shown as log2 fold change over the average of vehicle treated tumors.

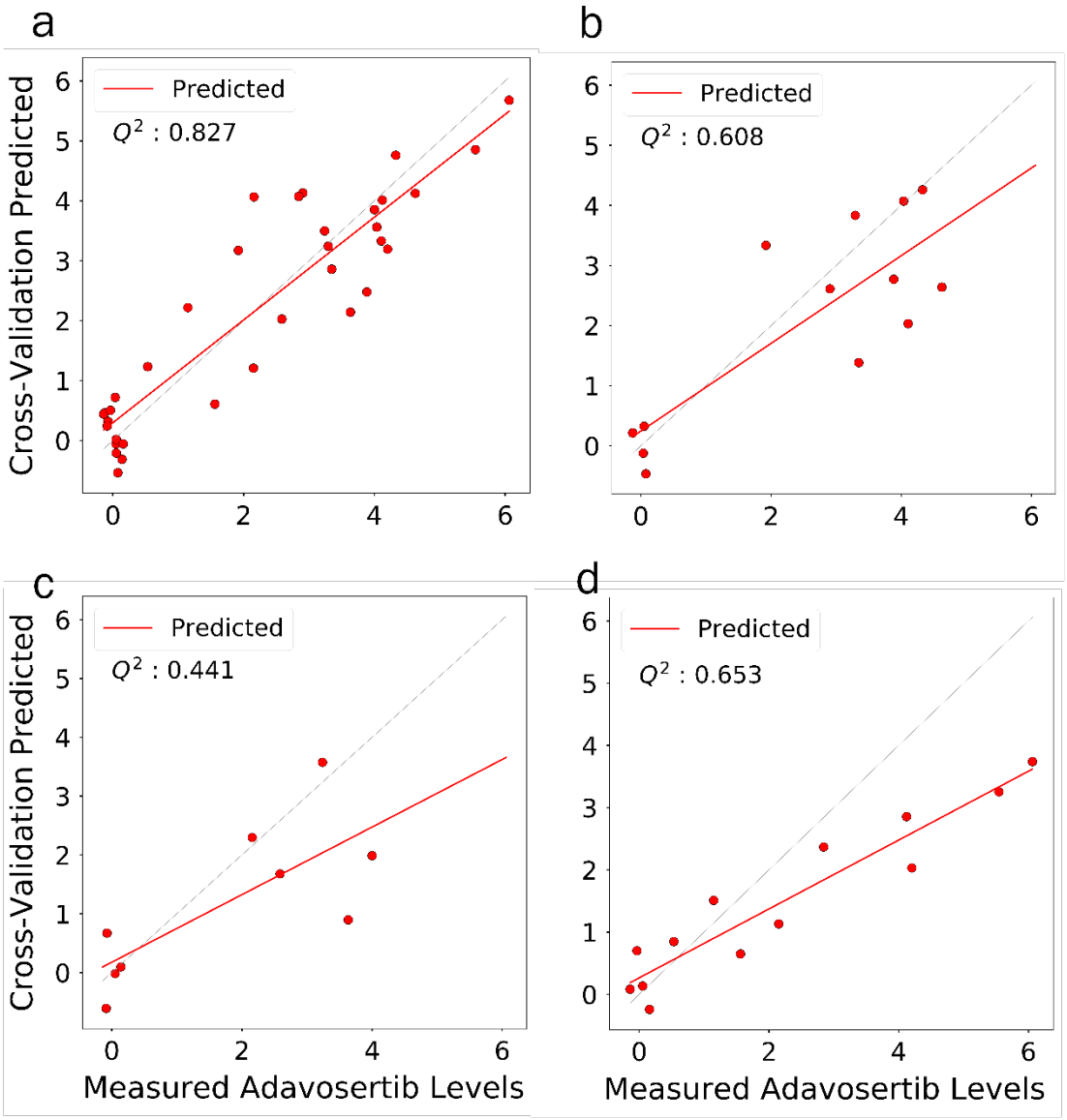

Supplementary figure S5. Cross validation of PLSR models. a) Correlation plots of measured and predicted adavosertib levels for 'cross-model' model built with data from all three PDX lines. Correlation plots of measured and predicted adavosertib levels cross-validated by holdout

methods where tumors from two PDX lines were used as a training set to predict drug levels of b) GBM12 c) GBM22 and d) GBM84 lines.

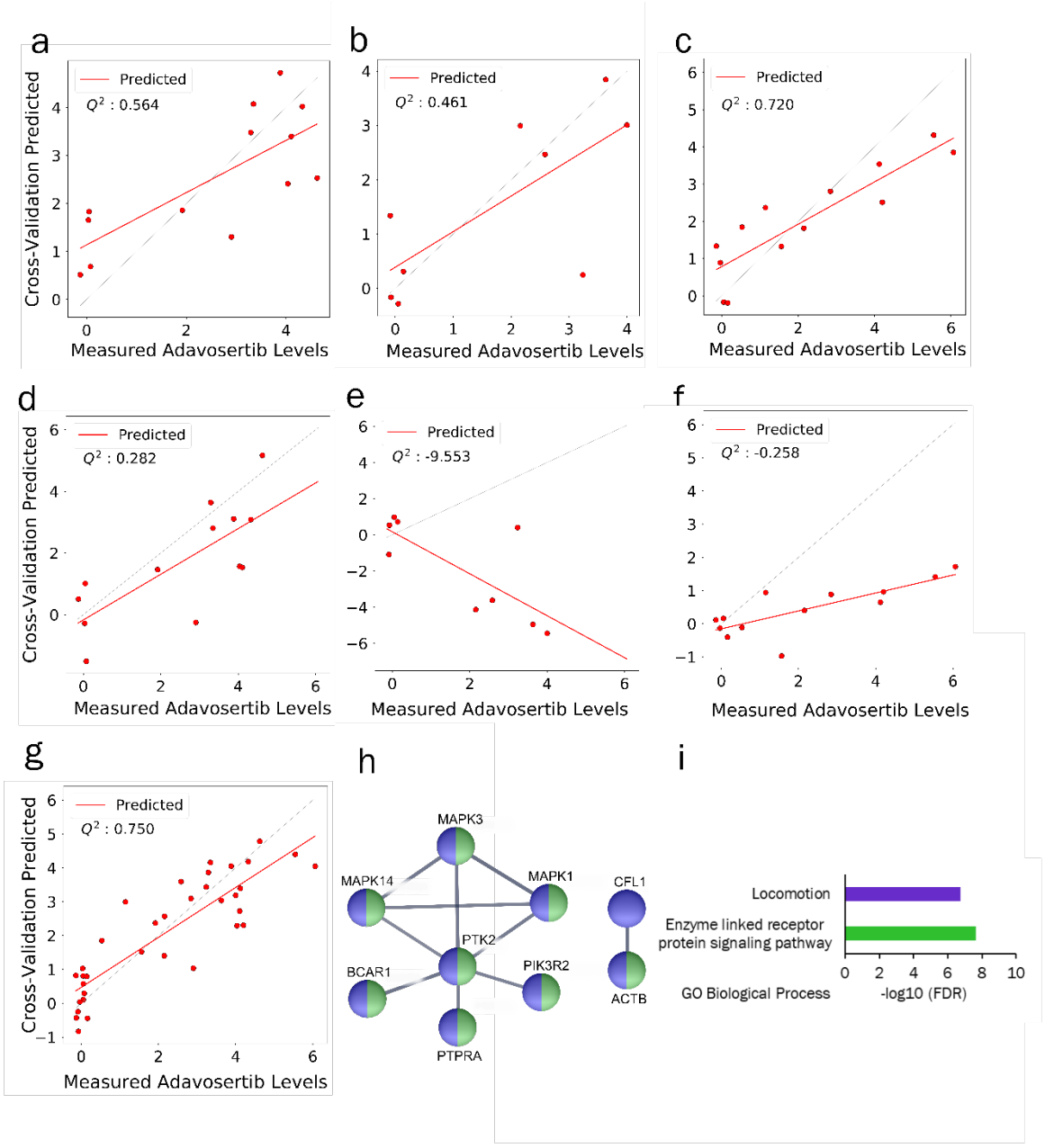

Supplementary figure S6. Phosphotyrosine response to adavosertib treatment in GBM PDXs. Correlation plots of measured and predicted adavosertib levels using pY data for a) GBM12, b) GBM22, c) GBM84, d-f) holdout methods where tumors from two PDX lines were used as a training set to predict drug levels of d) GBM12, e) GBM22, and f) GBM84 lines, g) cross model for all three lines with leave-one-out cross validation. h) Interaction network of phosphoproteins

based on STRING for members of cluster in Figure 4b. i) Enrichment of GO biological process for proteins in e.

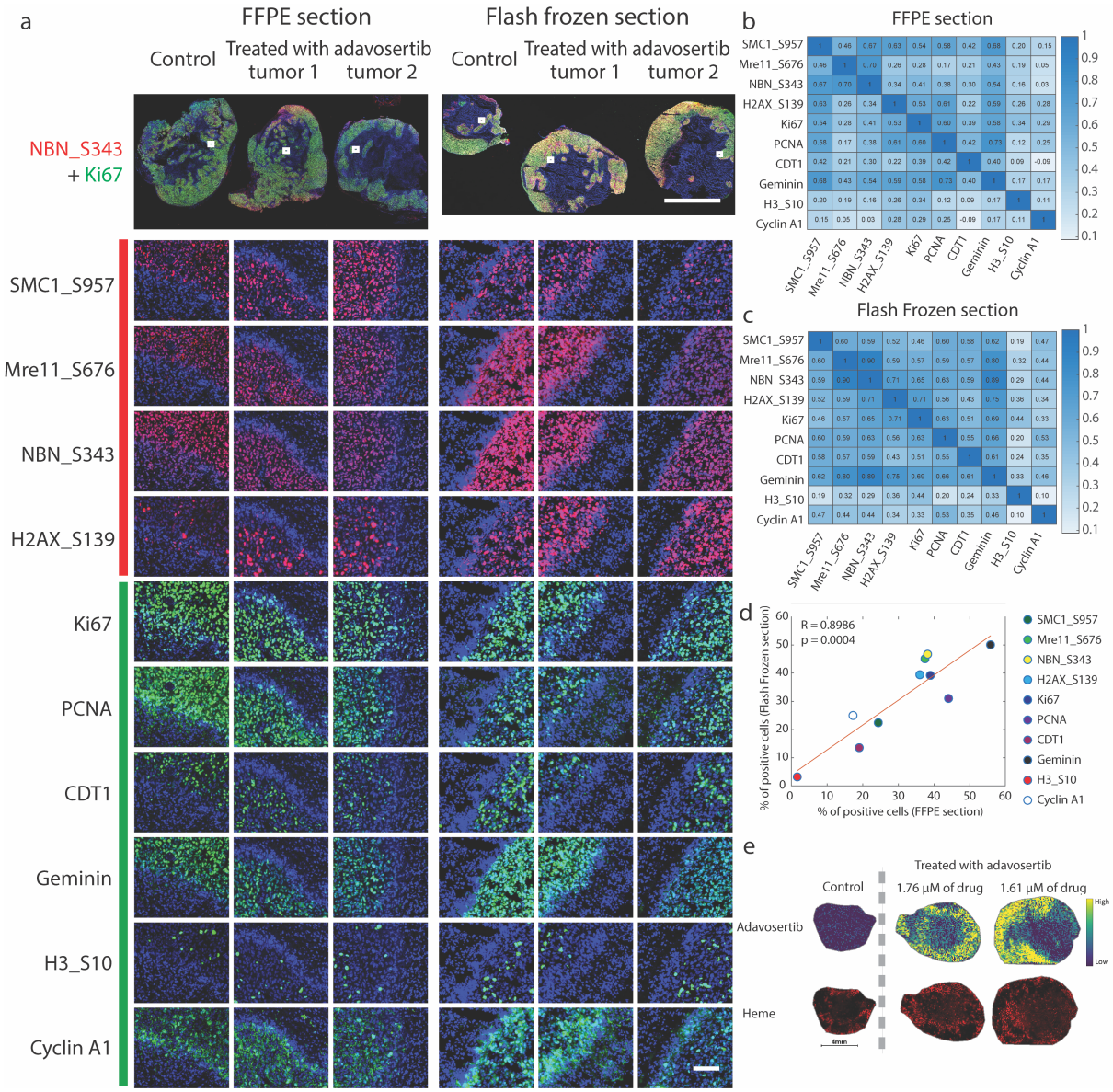

Supplementary figure S7. Validation of t-CyCIF comparing FFPE and FF specimens of the same tumor from a GBM22 PDX line, considering samples treated with 50 mg/kg of adavosertib and vehicle. Both FFPE section and frozen section were made from same PDX line derived from GBM22 batch 1 (control, n = 1; adavosertib high dose, 50 mg/kg, n = 2). The t-CyCIF antibody panel included DNA damage markers, SMC1_S957, Mre11_S676, NBN_S343, H2AX_S139, as well as cell cycle related markers Ki67, PCNA, CDT1, Geminin, H3_S10, and Cyclin A1. a) The representative t-CyCIF images of 10 antibodies from both FFPE and FF sections (scale bar: 5000um, montage; 100um, gallery images). b) The linear correlation coefficient between each

antibody at the single cell level was calculated in FFPE sections and c) FF sections. d) The percentage of positive cells for each marker was calculated in FFPE section and frozen section by manual gating method, and the scatter plot is presented. e) Distribution of adavosertib and heme on a serial FF section to the one used for CyCIF validation.

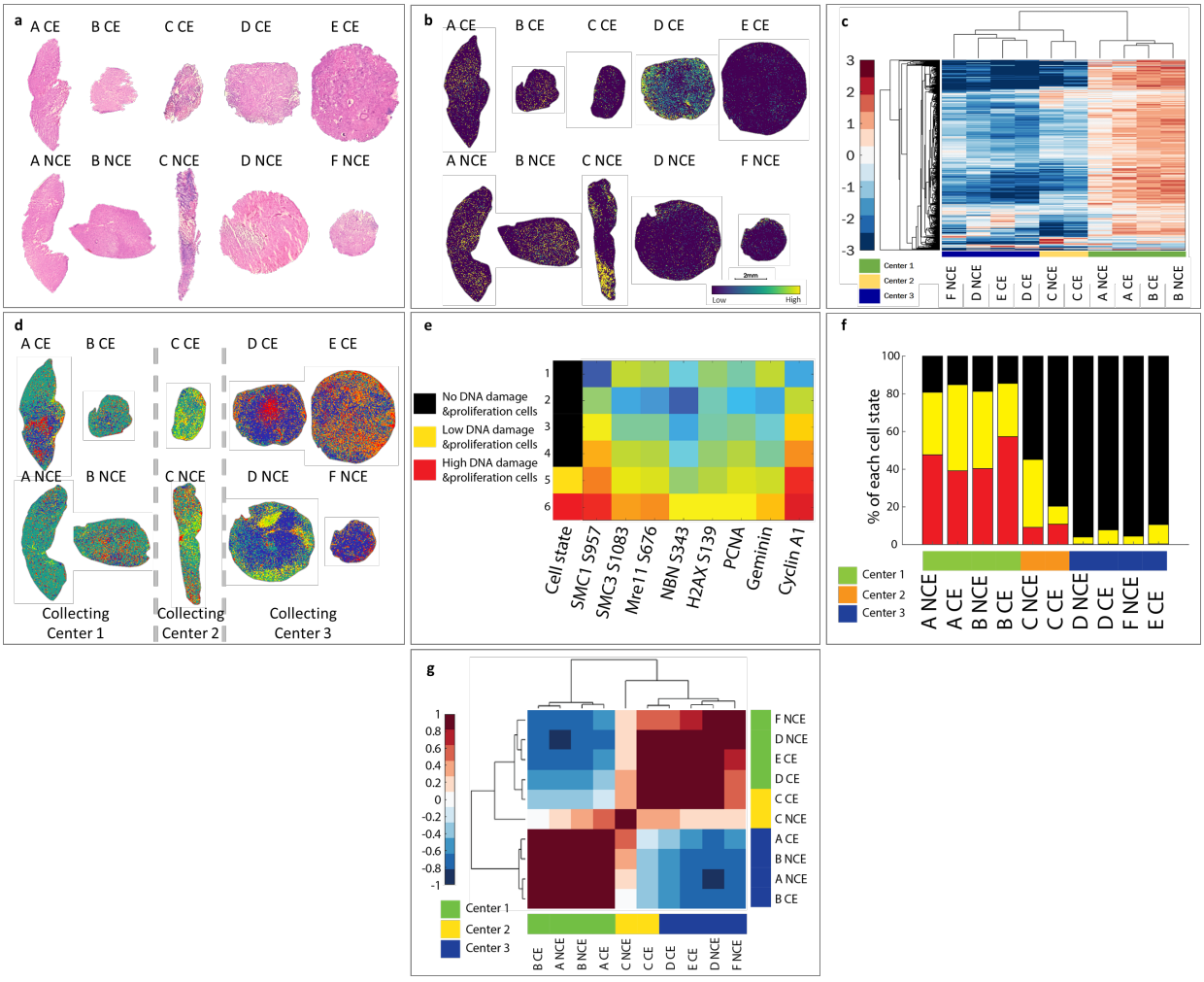

Supplementary figure S8. Integration of the multimodal platform for drug distribution and response using phosphoproteomics, MALDI-MSI and t-CyCIF on clinical specimens of GBM shows the batch effect clustering according to clinical collecting centers. a) Histological images of the clinical specimens show areas with high tumor cell density and necrotic areas which varied between patients; b) Distribution of adavosertib (*m/z* 501.2706) on serial sections of the same clinical specimens from CE and NCE regions. For most patients, similar drug intensity was found in CE and NCE specimens from the same individual. In case C, the drug intensity of the CE specimen was lower than that of the NCE specimen, probably due to necrotic areas and small regions with viable cells in the CE region compared to larger viable tumor regions found in the corresponding NCE specimen; c) HCA heatmap displaying phosphorylation levels of pSQ/pTQ sites assessed by phosphoproteomics; three clusters are observed based on the collecting center. Phosphorylation levels are log2 mean normalized. d) Segmentation map by bisecting k-means based on the biochemical fingerprints obtained by MALDI FT-ICR MSI. Regions with similar composition are represented with the same color. 7 clusters separate samples based on their collecting site; e) Characterization of t-CYCIF represented by the heatmap of

each cell population (clusters) using k-means clustering from all cells in frozen sections of the clinical specimens using 5 DNA damage related markers (SMC1_S957, SMC3_S1083, Mre11_S676, NBN_S343, and H2AX_S139) and 3 cell cycle related markers (PCNA, Geminin and Cyclin A1) (Heatmap: Red – high expression; blue – low expression). All cells were clustered into the following cell states: No DNA damage & proliferation cells (black, cluster 1-4); Low DNA damage & proliferation cells (yellow, cluster 5); High DNA damage & proliferation cells (red, cluster 6); f) The percentage of each cell population relative to all cells is presented as bar graph for each clinical trial sample; g) HCA heatmap based on the proportion of the clusters of the cell states.

The integration of multimodality data acquired from specimens originating from multi-site clinical studies, where uncontrolled sources of variability are much greater than with mouse models, can be challenging. We observed discrepancies attributable to clinical site-related batch effects, likely arising from different collection methods at the three participating medical centers. These results highlight the need for a stringent standardized sample collection procedure, including ischemia time between surgical biopsy and flash freezing of the specimen[18]. The use of Harmony integration, a widely used tool developed for single cell RNA sequencing analysis[14] on the t-CyCIF markers at a cellular level followed by linear mixed effect modeling to associate Harmony clusters with drug levels, accounted for individual donors with random effects.

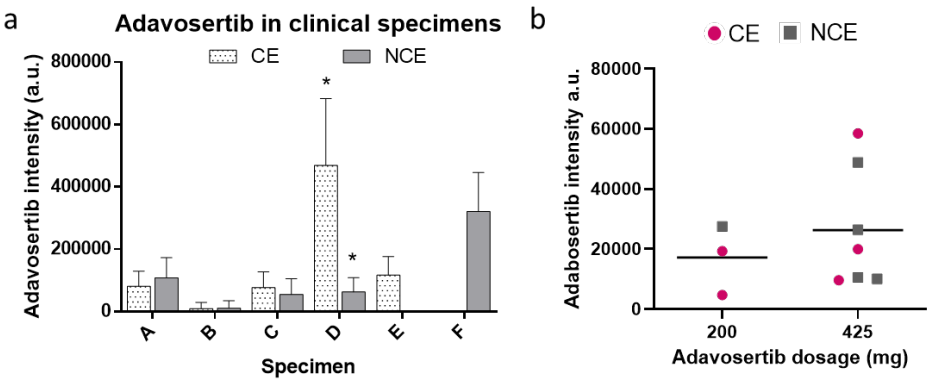

c

	Sample	Heme	Cer(d34:1)	ATP	Myristoyl-carnitine	Correlation coefficient drug-heme
a	CE					7.01E-04
	NCE					3.06E-05
b	CE					3.69E-04
	NCE					1.74E-03
c	CE					3.38E-03
	NCE					1.46E-02
d	CE					1.17E-01
	NCE					1.06E-02
e	CE					4.44E-03
f	NCE					7.25E-02

Supplementary figure S9. Tissue drug levels per dosage and region and MALDI FT-ICR MS images of the clinical specimens. a) Plot of the drug intensities found on the clinical specimens with their corresponding standard deviation shows heterogeneity in the distribution of adavosertib. Only specimen D showed significant differences between CE and NCE regions; b) plot of the drug intensities by dosage of adavosertib and discriminating by CE and NCE regions, showing no significant differences between the dosages; c) From left to right: distribution of heme (red), cer(d34:1), ATP and myristoyl-carnitine with high intensity represented in yellow and low intensity in blue. Correlation coefficients between heme and drug are in the last column, showing no correlation between them.

Supplementary table 1. Summary of phosphoproteomic data. Few identified phosphopeptides may reflect same phosphosites if multiple proteoforms or miscleaved peptides were detected. The PRIDE accession number is available in the Data Availability section.

Condition	Number of phosphopeptides	Number of phosphosites	Number of proteins
GBM12_pSQTQ	588	501	374
GBM22_pSQTQ	644	515	359
GBM84_pSQTQ	699	566	426
GBM12_pTyr	408	363	269
GBM22_pTyr	311	279	203
GBM84_pTyr	443	396	275
Clinical_pSQTQ	669	544	385

Supplementary table 7. Precision and accuracy of the method used to quantify flank drug concentrations using MALDI FT-ICR-MSI, considering three concentration levels: low (1 μM), medium (10 μM) and high (20 μM) of five replicates of tissue mimetic homogenate spiked with different drug concentrations between 1-20 μM.

	ACCURACY (n=5)	PRECISION (n=5)
Concentration (μM)	Recovery (%)	Repeatibility RSD (%)
1	100.71 ± 31.75	31.53
10	104.28 ± 17.93	17.20
20	98.73 ± 12.86	13.03